

Review

General Framework of Pressure Effects on Structures Formed by Entropically Driven Self-Assembly

Takashi Yoshidome

Institute of Advanced Energy, Kyoto University, Uji, Kyoto 611-0011, Japan;
E-Mail: t-yoshidome@iae.kyoto-u.ac.jp; Tel. +81-774-38-4695; Fax: +81-774-38-4695

Received: 1 March 2010; in revised form: 30 May 2010 / Accepted: 18 June 2010 /

Published: 23 June 2010

Abstract: We review a general framework of pressure effects on the structures formed by entropically driven self-assembly (for example, denaturation of proteins from their native structure and dissociation of ordered structure of the amyloid fibril occur at high pressures). In the framework, the translational entropy of water is an essential factor. Our findings are as follows: at low pressures, the structures almost minimizing the excluded volume (EV) generated for water molecules are stable. On the other hand, at high pressures, the structures possessing the largest possible water-accessible surface area together with sufficiently small EV become more stable. These characteristics are consistent with experimental observations.

Keywords: water; translational entropy; pressure denaturation of proteins; dissociation of protein complexes caused at high pressures; pressure-induced helix-coil transition of alanine-based peptides

PACS Codes: 82.60.Lf; 87.15Zg

1. Introduction

A variety of self-assembly processes have been observed in biological systems [1]. The most fundamental example of such processes is the folding of proteins into their unique native structures in aqueous solution under physiological conditions. It has also been recognized that protein complexes are often formed by aggregation of proteins. An example is the amyloid fibril, which is a fibril-like aggregation of misfolded or denatured proteins [1]. However, the stability of the native structure and

the ordered structures formed by folding and aggregation is strongly dependent on the thermodynamic variables such as pressure and temperature. Elucidation of the major factor governing the stability of these structures will provide physical insights into the mechanism of the biological self-assembly processes. In the present review, we focus on pressure effects on the stability of these structures.

It has been observed in experiments that denaturation of the native structure (pressure denaturation) [2-6] and dissolution of amyloid-fibrils [7-9] and virus assemblies [10] occur at high pressures. A common feature of these phenomena is that the volume change upon the pressure denaturation and dissociation is negative [3,6,10,11]. These pressure effects have often been discussed in terms of the Le Châtelier principle, which states that a pressure increase will shift a given equilibrium to the side that occupies the smallest volume [3,6,9]. Although this discussion is simple, the microscopic mechanism of pressure effects on the structures formed by biological self-assembly processes is still unclear.

The characteristics of the pressure-denatured structure of a protein have been analyzed in detail [2,4-6,12-16]. For example, the pressure dependence of the radius of gyration, R_g , of staphylococcal nuclease has been studied using synchrotron X-ray small-angle scattering [2] and small-angle neutron scattering [5]. The application of high pressure leads to an approximate twofold increase of R_g of the native structure. However, it is still much smaller than that of the random-coil structure [2]. In addition, some degree of β -like secondary structure is retained, even above 300 MPa [2], indicating that the pressure-denatured structure is different from the random-coil structure. Some authors have suggested that water has to penetrate into the protein interior to explain the experimental results [4,5,16]. The penetration of water into the protein interior has been observed using molecular dynamics (MD) simulations [13-15]—the number of the water molecules in the protein interior increases as the pressure becomes higher. According to these results, we can conclude that the pressure-denatured structure is characterized by swelling, water penetration into the protein interior, and only a moderate reduction of the compactness [6].

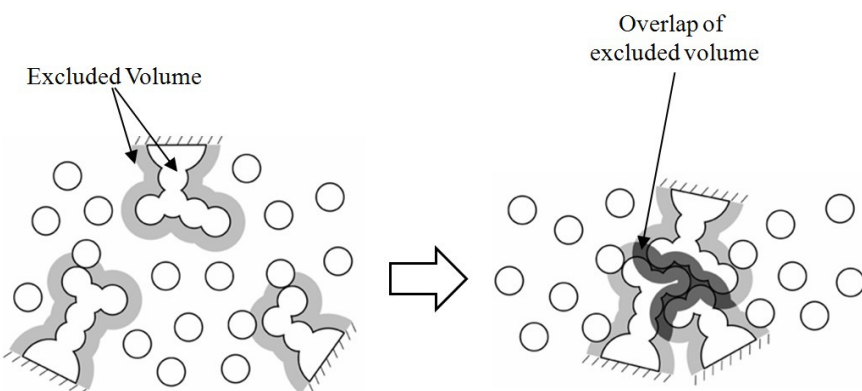
A puzzling result has recently been reported by Kato *et al.*, who analyzed the pressure effect on the helix-coil transition of alanine-based peptides using FTIR spectroscopy [17,18]. They showed that the fraction of the helix increases as the pressure becomes higher. Namely, the helix state is more stable than the coil state at high pressures. The volume of the helix is smaller than that of the coil state. The experimental result by Kato *et al.* appears to be inconsistent with the pressure denaturation or dissociation caused at high pressures known for many proteins because their result indicates that the peptides adopt the compact helix structure at high pressures. We note that Paschek *et al.* [19] have performed MD simulations for an α -helical peptide with an explicit solvation method and obtained results that are opposite to those of Kato *et al.*—the helix state becomes less stabilized by an increase in the pressure and the volume of the helix state is larger than that of the coil state, indicating that the coil state is more favored at high pressures.

Therefore, the picture which describes the pressure effects on the structures formed by biological self-assembly processes must explain all of the three experimental results: pressure denaturation of proteins, dissociation of protein aggregation, and pressure effect on the helix-coil transition of alanine-based peptides. The physical mechanism of pressure denaturation is often discussed in terms of the pressure dependence of the hydrophobicity. Using an information theory model of hydrophobic

interactions, Hummer *et al.* showed that stability of the contact configuration of two methane molecules relative to a water-mediated one decreases with rising pressures [16]. Based on this result it is concluded that the weakening of the hydrophobic interactions between nonpolar side chains is the major cause of pressure denaturation [6,20]. However, the experimental results of alanine-based peptides [17,18] cannot be explained in terms of the weakening of the hydrophobicity for the following reason. In the conventional view of the hydrophobicity [21], the water adjacent to a nonpolar group is entropically unstable, and this effect drives the solvent-accessible surface area (ASA) of nonpolar group to decrease (here, the ASA is the area of the surface that is accessible to the centers of solvent particles [22]). We have confirmed that for the helix structure composed of 20 alanines the ASA of the side chains remains almost unchanged upon the transition from the coil state to the helix state. Therefore, the transition of alanine-based peptides from the coil state to the helix state cannot be elucidated by the conventional hydrophobic effect. The transition does not follow the weakening of the hydrophobicity at high pressures. Therefore, a unified picture explaining all three experimental results described above is not provided by the notion of a weakening of the hydrophobicity. A breakthrough is not likely to be obtained unless a novel concept is employed.

Recent theoretical studies based on the statistical thermodynamics of fluids have shown that the translational entropy of water is a principal driving force in a variety of biological self-assembly processes such as protein folding [23–28], molecular recognition between guest ligands and host enzymes [27,29,30], and aggregation of protein molecules like the amyloid fibril [27,31,32]. We first note that the presence of proteins generate an excluded volume (EV) which the centers of water molecules cannot enter [23,24]. Upon the self-assembly processes, the EV is largely decreased by the overlap of EV (see Figure 1), leading to an increase in the total volume available to the translational displacement of water molecules.

Figure 1. Schematic representation of three side chains. The excluded volume generated by a side chain is the volume occupied by the side chain itself plus the volume shown in gray. When side chains are closely packed, the excluded volumes overlap, leading to a gain of the water entropy.



Thus, the formation of the self-assembly leads to increases in the number of accessible configurations arising from the translational displacement of water molecules and in the water entropy. In the entropically driven self-assembly at ambient pressure and temperature, the structures almost minimizing the EV for water molecules are stabilized. Experimental studies support the present

picture: it has been shown that in protein folding [33], receptor-ligand binding [34], amyloid-fibril formation [35], association of virus [10], and formation of actin filaments [36,37] the enthalpic and entropic changes are both positive at ambient temperature and pressure, proving that these processes are entropically driven.

From a viewpoint of water-entropy effect, one might think that the native structure and the ordered structure formed by aggregation would be further stabilized by applying a higher pressure. However, as shown by experiments, this is not the case. It is interesting to study whether the pressure effects on the structures formed by entropically driven self-assembly can also be explained in terms of the translational entropy of water. In the present review, we present the general framework of pressure effects on the structures formed by entropically driven self-assembly from a fairly general viewpoint [38]. In the framework, the translational entropy of water is an essential factor (our concern is to elucidate why the structures formed by the entropically driven self-assembly dissociate at high pressures, although from the viewpoint of the translational entropy of water the structure with small EV seems to be even more stable at high pressures. Highly charged or natively unfolded proteins are excluded from the discussion because the water-entropy effect is weaker than the other effect such as the solute-solvent interaction energy).

The outline of the present review is as follows. We first briefly describe the studies on pressure denaturation of proteins by Harano and Kinoshita [39,40] (Section 2). The models of solute and solvent, and the theoretical approach are shown in Section 3. We show the following general feature of the structures at low and high pressures in Section 4: at low pressures, the structural stability can be argued in terms of the EV. On the other hand, the structures possessing the largest possible solvent-accessible surface area (ASA) together with sufficiently small EV turn more stable at high pressures. As an illustration of the present picture, we discuss two examples, pressure denaturation of a protein [38] and pressure-induced helix-coil transition of a polypeptide [41]. We also comment on the dissolution of amyloid fibrils caused at high pressures in terms of the translational entropy of water [38]. Final conclusions are drawn in Section 5.

2. Driving Force of Pressure Denaturation of Proteins: Translational Entropy of Water

The free energy change upon denaturation can be described as follows:

$$\Delta G = \Delta E_I + \Delta \mu - T\Delta S_C \quad (1)$$

where E_I is the protein intramolecular energy, μ is the solvation free energy which is the free-energy change by the insertion process of a solute into solvent, S_C is the conformational entropy of protein, and T is the absolute temperature. $\Delta B \equiv B_D - B_N$ denotes the change in a thermodynamic quantity B upon denaturation. The subscripts “N” and “D” represent the values for the native state and for the denatured state, respectively.

At ambient pressure, the native structure is stabilized and therefore ΔG is positive. For pressure denaturation to occur, ΔG must turn negative at high pressures. The change in the conformational entropy upon denaturation, $|\Delta S_C|$, is expected to be independent of the pressure or smaller at high pressures due to the constraint caused by the denser solvent [42]. Within the framework of classical mechanics, the intramolecular energy for any structure remains unchanged against a pressure change.

Thus, $\Delta\mu$ must decrease to a significant extent as the pressure P increases and eventually become negative for the denaturation to occur.

We also discuss the negative sign of the volume change, $\Delta V = (\partial\Delta G/\partial P)_T$ upon denaturation. According to the discussion in the previous paragraph, both of $(\partial\Delta E_l/\partial P)_T$ and $(\partial\Delta S_c/\partial P)_T$ are non-negative, therefore, the sign of ΔV is determined by $(\partial\Delta\mu/\partial P)_T$. The partial molar volume (PMV), which is denoted by V_{PMV} , is the change of the system volume occurring upon the solute insertion in the isobaric process. Thermodynamically, the PMV is the pressure derivative of the solvation free energy expressed as:

$$V_{PMV} = (\partial\mu/\partial P)_T \quad (2)$$

The present discussion indicates that the change in PMV upon denaturation is negative ($\Delta V_{PMV} < 0$). The solvation free energy μ is the excess chemical potential of the solute in the fluid of interest and is the same, irrespective of the solute insertion process (isochoric or isobaric) [43]. We consider the isochoric process hereafter. Under the isochoric condition, the solvation free energy is given by $\mu = U - TS$ where U is the solvation energy and S is the solvation entropy (SE). It has been observed that nonpolar side chains are more separated in a denatured structure with water molecules penetrating its hydrophobic core [5,14-16]. When the penetration occurs, the breakage of hydrogen bonds of water is unavoidable, leading to a loss in terms of the solvation energy. There must be an even larger gain in terms of the solvation entropy, a dominant increase in the solvent entropy.

Harano and Kinoshita have made a statistical-mechanical analysis of pressure denaturation of a protein using the three-dimensional (3D) integral equation theory [39,40]. To focus on the translational entropy of water, the protein is modeled as a set of fused hard spheres and water is taken to be hard spheres. Their results are as follows: at high pressures the water entropy becomes higher when the protein takes a specific unfolded structure. The unfolded structure is moderately less compact than the native structure (*i.e.*, the EV is only moderately larger; see Table 1) and characterized by the cleft and/or swelling and solvent penetration into the interior [39,40] (hereafter we refer to this structure as the “swelling structure”). The change in the PMV upon denaturation to this unfolded structure is negative [39,40]. These characteristics are consistent with the experimental observations [3,5,6] and they concluded that the pressure denaturation is driven by the translational entropy of water.

Table 1. Values of excluded volume (EV) and solvent-accessible surface area (ASA) for native, swelling, and random-coil structures of protein G [38,42]. Those of the random-coil state are the average for 32 structures.

	EV (Å ³)	ASA (Å ²)
Native	11,600.3	3,670.90
Swelling	11,926.9	4,210.81
Random coil	14,002.9	5,947.13

It is, however, difficult to give an interpretation of the results in terms of the translational entropy of water because the EV of swelling structure is larger than that of the native structure. It appears that the native structure with almost the smallest EV seems to become more stable as the pressure increases. For example, within the framework of the Asakura-Oosawa (AO) theory [44,45], which is widely used

as a simple way of understanding the EV effect, the entropic gain upon a self-assembly is given by $-k_B\rho_S\Delta V_{ex}$ where k_B is the Boltzmann constant, ρ_S the solvent density, $\Delta V_{ex} (< 0)$ the decrease in the EV. Since ρ_S becomes higher as the pressure increases, the structures with small EV should further be stabilized by applying high pressures. This statement clearly conflicts with the theoretical results [39,40] as well as the experimental observations [6]. It is also unclear whether the other phenomena such as the dissolution of amyloid fibril occurring at high pressures can also be explained in terms of the translational entropy of water. To solve these problems, we employ the morphometric approach described in the next section.

3. Models and Theoretical Approach for the Calculation of Solvation Thermodynamic Quantities

3.1. Models

To focus our analysis on the entropic effect, we employ the hard-body model system: the solvent particles are modeled as hard spheres with diameter $d_S = 2.8 \text{ \AA}$ that is the molecular diameter of water, and the solutes (proteins and polypeptides) are modeled as a set of fused hard spheres. In this model system, all the configurations share the same energy and the system behavior is purely entropic in origin. The polyatomic structure, which is crucially important, is accounted for on the atomic level. The (x, y, z) coordinates of all the protein or polypeptide atoms (hydrogen, carbon, nitrogen, oxygen, etc.) in the backbone and side chains are taken into consideration.

In the present review, we focus on the SE S and the PMV V_{PMV} . The validity of the hard-body model in calculating S and V_{PMV} has been shown in the previous papers [40,46]. For example, Imai *et al.* have considered the native structures of a total of eight peptides and proteins and calculated S using the three-dimensional reference interaction site model (3D-RISM) theory combined with the all-atom potentials and SPC/E water model [46]. Even when the protein-water electrostatic potentials, which are quite strong, are shut off and only the Lennard-Jones potentials are retained, S only decreases by less than 5%. Further, an approximate value of S can be obtained even by using the 3D integral equation theory [29,31,47] combined with the hard-body model. For example, $-TS$ of human erythrocyte ubiquitin (PDB code: 3EBX) is 1,802 kcal/mol when the 3D-RISM theory combined with the all-atom potentials is applied, and it is 1,882 kcal/mol when the 3D integral equation theory combined with the hard-body model is applied [46]. This is because the contribution to the SE from the water molecules near the protein is much smaller than that from those in the system [26].

We note that in general, the solvation energy is largely dependent on the solute-water interaction potential, while the SE is not. The hydration free energy μ , entropy S_{VH} , and energy U_{VH} under the isochoric condition are calculated for a spherical solute with diameter 2.8 Å using the angle-dependent integral equation theory [48,49] combined with the multipolar water model [50,51] (when the solvent is water, the solvation free energy, entropy, and energy are referred to as the hydration free energy, entropy, and energy, respectively). This theory combined with the multipolar water model can reproduce well the experimental observations such as the dielectric constant of bulk water [48] and the hydrophobic [48] and hydrophilic [49] hydrations. For the hard-sphere solute with zero charge, the calculated values are $\mu = 5.95k_B T$, $S_{VH} = -9.22k_B$, and $U_{VH} = -3.27k_B T$ [28]. When the point charge $-0.5e$ (e is the electronic charge) is embedded at its center, the calculated values are $\mu = -32.32k_B T$,

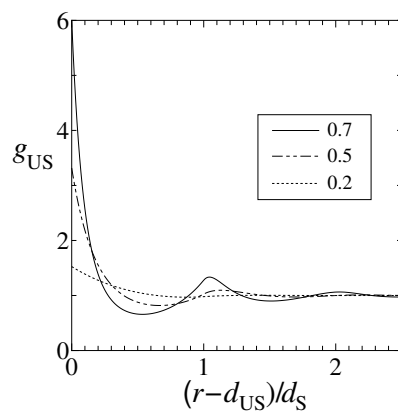
$S_{\text{VH}} = -10.11k_B$, and $U_{\text{VH}} = -42.43k_BT$ [28]. Thus, S_{VH} is fairly insensitive to the solute-water interaction potential while μ and U_{VH} are largely influenced by it. This gives another justification of the protein model, a set of fused hard spheres.

Harano and Kinoshita [40] have obtained the values of V_{PMV} of five different proteins in accordance with the Kirkwood-Buff formulation [52]:

$$V_{\text{PMV}} = \iiint \{1 - g_{\text{us}}(x, y, z)\} dx dy dz \quad (3)$$

where $g_{\text{us}}(x, y, z)$ represents the microstructure of the solvent near the protein surface and is referred to as the reduced density profile (hereafter, the subscripts, “S” and “U”, respectively, represent “solvent” and “solute”). It has the physical meaning that the number of solvent molecules within the volume element $dx dy dz$ is given by $\rho_S g_{\text{us}}(x, y, z) dx dy dz$. $g_{\text{us}}(x, y, z)$ is calculated using the 3D integral equation theory combined with the hard-body model. The values of the PMV obtained are in accord with the experimentally measured values. For example, the PMV of lysozyme (PDB code: 1HEL) calculated is $11,600 \text{ cm}^3/\text{mol}$ that is in good agreement with the average of the experimentally measured value, $10,100 \text{ cm}^3/\text{mol}$ [40].

Figure 2. Reduced density profiles of hard-sphere solvent near a hard-sphere solute $g_{\text{us}}(r)$ at $\rho_S d_S^3 = 0.2$ (dotted line), $\rho_S d_S^3 = 0.5$ (2-dot dashed line), and $\rho_S d_S^3 = 0.7$ (solid line).



This result has been interpreted as follows [27]. We divide the term in the right hand of Equation (3) into the integrations inside and outside the core region. Inside the core region, due to the overlap of the protein and solvent, the protein-solvent potential is infinitely large and $g_{\text{us}} = 0$. It follows that the integration inside the core region equals the EV, V_{ex} , which the centers of solvent molecules cannot enter. The integration outside the core region takes a negative value because a layer within which the solvent density is higher than in the bulk is formed near the protein surface due to the packing force arising from the translational displacement of solvent molecules [40] (g_{us} of hard-sphere solvent near a hard-sphere solute is shown in Figure 2 as an example). Since the higher density is almost limited to the first layer (*i.e.*, the thickness of the denser layer reaches only about half of the solvent diameter), the integration outside the core region is roughly in proportion to the solvent-accessible surface area (ASA) denoted by A . Thus, we can write:

$$V_{\text{PMV}} \sim V_{\text{ex}} - \xi A \quad (4)$$

(in a strict sense, V_{PMV} is affected not only by these two terms but also by the curvature terms as described in Section 3.2) The parameter ξ is related to the average solvent density within the dense layer. A hydrophilic group in the protein makes a large, positive contribution to ξ because $g_{US} \gg 1$ on an average near it [49]. By contrast, near a group which is hydrophobic enough to overcome the packing force, $g_{US} \sim 1$ or $g_{US} < 1$ [49], with the result that the group makes a small, negative contribution to ξ . Since hydrophilic and hydrophobic groups are almost irregularly distributed on the protein surface, the overall value of ξ becomes positive, and V_{PMV} is smaller than V_{ex} . When the protein is modeled as a fused hard spheres and water is taken to be hard spheres, the water density near a hydrophilic group is underestimated while that near a hydrophobic group is overestimated, leading to a fortuitous cancellation of errors and a better result.

3.2. Morphometric Approach

In the morphometric approach [53,54], the solvation thermodynamic quantities Z (S/k_B and V_{PMV}) are expressed using only four geometric measures of a complex (polyatomic) solute with a fixed structure and corresponding coefficients. The resultant expression is:

$$Z = C_1 V_{ex} + C_2 A + C_3 X + C_4 Y \quad (5)$$

The four measures are the EV (V_{ex}), the ASA (A), and the integrated mean and Gaussian curvatures of the accessible surface (X and Y) respectively. The water-accessible surface is the surface that is accessible to the centers of water molecules [22]. A , X , and Y are the surface area and the integrated curvatures of the water-accessible surface. The EV is the volume that is enclosed by the water-accessible surface area.

In this approach, the solute shape enters Z only via the four geometric measures. Therefore, the four coefficients ($C_1 - C_4$) can be determined in a simple geometry. They are determined from the solvation thermodynamic quantities calculated for hard-sphere solutes with various diameters immersed in the hard-sphere solvent. The morphometric form applied to hard-sphere solutes reduces to:

$$Z = C_1 \{(4\pi/3)d_{US}^3\} + C_2(4\pi d_{US}^2) + 4\pi C_3 d_{US} + 4\pi C_4 \quad (6)$$

where $d_{US} = (d_U + d_S)/2$ and d_U is the solute diameter. The four coefficients are determined using the least squares fitting to Equation (6). Once the four coefficients are determined, solvation thermodynamic quantities for a solute with a fixed structure are obtained by calculating only the four geometric measures.

The solvation free energy μ of hard-sphere solute immersed in the hard-sphere solvent is obtained in accordance with the Morita-Hiroike formula [55,56]:

$$\mu = 4\pi\rho_S \int \{h_{US}(r)^2/2 - h_{US}(r)c_{US}(r)/2 - c_{US}(r)\} r^2 dr \quad (7)$$

where $h_{US}(r)$ and $c_{US}(r)$ are the total and direct correlation functions between the hard-sphere solute and hard-sphere solvent, respectively ($g_{US}(r)$ is $h_{US}(r)+1$). The integration range is from 0 to ∞ . In the hard-body model, μ is equal to $-TS$. The PMV is obtained using Equation (3). The correlation functions are calculated using the integral equation theory, elaborated statistical thermodynamics theory [38,43].

It has been shown that S and V_{PMV} calculated by the 3D integral equation theory [29,31,47] applied to the hard-body model can be reproduced with sufficiently high accuracy by the morphometric approach applied to the same hard-body model [41,54]. For example, the deviation of the SE by the morphometric approach from that obtained by the 3D integral equation theory is less than $\pm 2\%$ [54]. V_{PMV} of the complete α -helix structure composed of 20 alanines at $\rho_{SDS}^3 = 0.7$ is $94d_S^3$ when the morphometric approach is applied, and it is $90d_S^3$ when the 3D integral equation theory is employed [41]. The high accuracy also indicates that the SE obtained using the all-atom potential and the PMV experimentally observed can well be reproduced by the morphometric approach applied to the hard-body model (in Section 3.3 we also show that the experimentally measured change in thermodynamic quantity upon apoplastocyanin folding is quantitatively reproduced using the morphometric approach).

Computation time required in the morphometric approach is over four orders of magnitude shorter than that required in the 3D integral equation theory: The calculation for one structure of protein G is finished in less than 1 sec on a small personal computer [54]. In principle the coefficients can be determined via any route: for example, the angle-dependent integral equation theory [48,49] combined with the multipolar water model [50,51] and a computer simulation using the SPC/E model [57] for water. However, the approach is applicable only when the solute-solvent interaction potential includes no electrostatic part [26]. There is no problem in the present case where a protein can be modeled as a set of fused hard spheres.

3.3. Quantitative Comparison between Experimental and Theoretical Results for Apoplastocyanin Folding

Terazima *et al.* developed a novel experimental technique which enables us to directly measure the enthalpic change and the system-volume change upon protein folding at 298K [33]. They showed that during apoplastocyanin (apoPC) folding, the system-volume change is almost 0 and that folding accompanies an enthalpic loss of 870 kJ/mol that is very large. It follows from the former result that the change in the hydration thermodynamic quantities of apoPC folding under the isobaric (constant-pressure) condition can be considered to be the same as those under the isochoric (constant-volume) condition. Thus, the change in the enthalpy change and the entropic change upon folding under the isobaric condition can be treated as the energy and entropy change upon folding under the isochoric condition. The latter result indicates that the folding leads to a great gain of the water entropy which surpasses the enthalpic loss and the conformational-entropy loss.

The water-entropy gain upon folding can be estimated as follows [25]: the free-energy gain upon the folding is given by “ $\Delta H - T(\Delta S + \Delta S_C)$ ” where ΔH is the enthalpy loss and ΔS_C is the conformational-entropy (CE) loss. We estimate ΔS_C via following two different routes.

One of the routes has been employed by Harano and Kinoshita [24]: The CE of the unfolded state is roughly estimated as follows. For the backbone, per residue there are two dihedral angles which can rotate and each angle has three stable values. Therefore, the number of possible combinations is $3^2 = 9$ and the contribution to the CE is $k_B \ln 9$. Based on the study by Doig and Sternberg [58], we regard the contribution from the side chain to the CE as $1.7k_B$ per residue. It is assumed that the CE of the native structure is essentially zero. The CE loss ΔS_C upon folding with N_r residues is expressed as:

$$\Delta S_C/k_B = -N_r(\ln 9 + 1.7) \quad (8)$$

However, the above route gives rise to a considerable overestimation of the CE loss. This is because many of the conformations counted undergo unrealistic overlaps of protein atoms, as is frequently encountered when the generation of unfolded structures is undertaken. The other route is based on the result from the experimental studies of Fitter using the neutron spectroscopy [59]. He estimated the temperature dependence of the radius parameter r which represents a length scale within which each residue can freely move. The CE loss is given by:

$$\Delta S_C/k_B = -3N_r \ln(r_u/r_f) \quad (9)$$

where r_u and r_f are the radius parameters for the unfolded state and for the folded state, respectively. The estimation of the radius parameters was made at three temperatures, 303K, 323K, and 343K. In order to estimate the CE loss at 298K, we first perform the linear fitting of the temperature dependence of r_u and r_f , and then obtain their values at 298K. The neutron scattering experiments cover mainly the picosecond time regime though the fluctuations in other time scales also affect the CE. For this reason, the use of Equation (9) results in a considerable underestimation of the CE loss. The actual CE loss should lie between the two values calculated from Equation (8) and Equation (9), respectively.

Since N_r of apoPC is 99, ΔS_C can be estimated to be in the range, $305 \text{ kJ/mol} < -T\Delta S_C < 956 \text{ kJ/mol}$ [25]. It is assumed that the free-energy gain takes the most probable value shared by a number of proteins, -50 kJ/mol [60]. Using $\Delta H = 870 \text{ kJ/mol}$, the water-entropy gain is estimated to be in the range, $-1876 \text{ kJ/mol} < -T\Delta S < -1225 \text{ kJ/mol}$.

We calculated the water-entropy gain upon folding of apoPC under isochoric condition using the morphometric approach [25]. The protein is modeled as a set of fused hard spheres. The four coefficients of S are determined from S calculated for hard-sphere solutes with various diameters immersed in the multipolar water model [50,51]. The values of S of hard-sphere solute are obtained using the angle-dependent version of integral equation theory [48,49] combined with multipolar water model [50,51]. It follows that the water-entropy gain upon folding of apoPC, $-T\Delta S$, is -1658 kJ/mol , which is certainly in the range estimated (we assume that the unfolded state is random-coil state [25]). Therefore, we succeeded in reproducing quantitatively the change in the thermodynamic quantity upon apoPC folding by our theoretical method.

By decomposing the water-entropy gain into several components, it is found that the translational-entropy gain is about 20 times larger than the rotational-entropy gain [25]. Thus, the translational-entropy gain of water is the major driving factor of folding of apoPC. According to the usual view [21], the water adjacent to a nonpolar group is entropically unstable (especially the rotation-entropy loss of water), and protein folding is driven by the release of such unfavorable water to the bulk through the burial of nonpolar groups. However, the entropic gain originating from this view is too small to elucidate the water-entropy gain manifesting the apoPC-folding data [25].

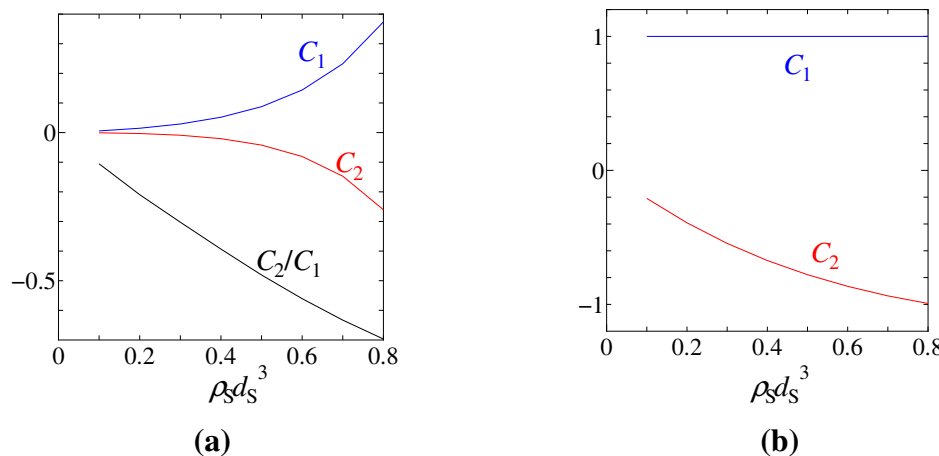
4. General Framework of Pressure Effects on Structures Formed by Self-assembly

We first discuss the pressure effects on the first and second coefficients in morphometric form for the SE and the PMV of hard-body system [C_3 and C_4 are not discussed here because in Equation (5) $C_3X + C_4Y$ is much smaller than $C_1V_{ex} + C_2A$.]. Figure 3(a) shows the density dependence (corresponding

to the pressure dependence) of the first and second coefficients, C_1 and C_2 , in the morphometric form applied to the SE, $-S/k_B$. It is found that C_1 and C_2 take positive and negative values, respectively, at any density. C_1 and $|C_2|$ increase remarkably with rising density, but the increase in the latter is larger: $|C_2|$ is much smaller than C_1 at low pressures, but they are comparable in magnitude at high pressures.

The positive value of C_1 can easily be interpreted as the solvent-entropy loss caused by the solute insertion. The basic physics to give an interpretation of the negative value of C_2 is in the phenomenon that when a large hard-sphere solute is immersed in small hard spheres forming the solvent, the small hard spheres are enriched near the solute despite that there are no direct attractive interactions between the solute and solvent particles and this enrichment becomes greater as the pressure increases (see Figure 2). We note that the presence of a solvent molecule generates an EV for the other solvent molecules in the system [39,40]. Due to this solvent crowding, part of the solvent particles is driven to contact the solute surface. The contact brings the overlap of the EVs generated by the solute and the solvent particles in contact with the solute. As a consequence, the total volume available to the translational displacement of the other solvent particles (*i.e.*, the solvent particles well outside the enriched layer in the vicinity of the solute) increases, leading to an entropic gain. Such an entropic gain becomes large when the solute takes the structure with large ASA. Therefore, C_2 takes negative value.

Figure 3. (a) $C_1 (\text{\AA}^{-3})$, $C_2 (\text{\AA}^{-2})$, and $C_2/C_1 (\text{\AA})$ of solvation entropy, $-S/k_B$, plotted against solvent density corresponding to the pressure. (b) C_1 and $C_2 (\text{\AA})$ of partial molar volume plotted against solvent density.



As for the density dependence of V_{PMV} [Figure 3(b)], C_1 is constant at the value corresponding to 1. The density dependence of $|C_2|$ is similar to that of $-S/k_B$ —it increases as the density is raised. The positive value of C_1 represents the increment of the volume of the system by the EV of the solute. The negative value of C_2 arises from the reduction of the EVs by the contact of the solute and the solvent particles. V_{PMV} is decreased as the ASA is increased.

Since C_3X+C_4Y is much smaller than $C_1V_{\text{ex}}+C_2A$, the difference in the solvation thermodynamic quantity Z between the structures stabilized at high and low pressures can approximately be described as follows:

$$Z^{\text{High}} - Z^{\text{Low}} \sim C_1(V_{\text{ex}}^{\text{High}} - V_{\text{ex}}^{\text{Low}}) + C_2(A^{\text{High}} - A^{\text{Low}}) \quad (10)$$

where the superscripts “High” and “Low” denote the structures stabilized at high and low pressures, respectively and Z is $-S/k_B$ or V_{PMV} . At high pressures, the structure formed by the entropically driven self-assembly is usually dissolved: the protein is unfolded and the amyloid fibrils are dissolved. $V_{ex}^{High} - V_{ex}^{Low}$ and $A^{High} - A^{Low}$ are, respectively, changes in the EV and the ASA upon the destruction, and they are both positive. We consider $-S/k_B$ for Z . For the pressure-induced destruction to occur, $C_2(A^{High} - A^{Low})$ (negative) must surpass $C_1(V_{ex}^{High} - V_{ex}^{Low})$ (positive) at sufficiently high pressures. In other words, only the structure making the former larger can be stabilized at elevated pressures. Such structure should have a largest possible ASA together with sufficiently small EV (hereafter, we refer to these as “pressure-induced structures”). The pressure dependence of the structural stability is determined by a subtle balance between these two terms. In the case of the PMV, $V_{ex}^{High} - V_{ex}^{Low}$ and $C_2(A^{High} - A^{Low})$ are positive and negative, respectively, and these signs are same as those of $-S/k_B$. $V_{PMV}^{High} - V_{PMV}^{Low}$ becomes negative when solute takes pressure-induced structure.

We can thus obtain the following general feature of the solute structure at the low and high pressures: at low pressures, the structures almost minimizing the EV are stable. On the other hand, at sufficiently high pressures, the stabilized structures, pressure-induced structures, are compact and characterized by the largest possible ASA together with the EV kept sufficiently small. The change in V_{PMV} upon the transition to the pressure-induced structures is negative.

In the following subsections, two examples—pressure denaturation of proteins and coil-helix transition of polypeptide at high pressures—are discussed to show the validity of the present picture. We also give a comment on the pressure-induced dissociation of amyloid fibrils. It should be emphasized here that $C_3X + C_4Y$ is fully incorporated in $-S/k_B$ and V_{PMV} in Sections 4.1 and 4.2.

4.1. Microscopic Mechanism of Pressure Denaturation of Proteins

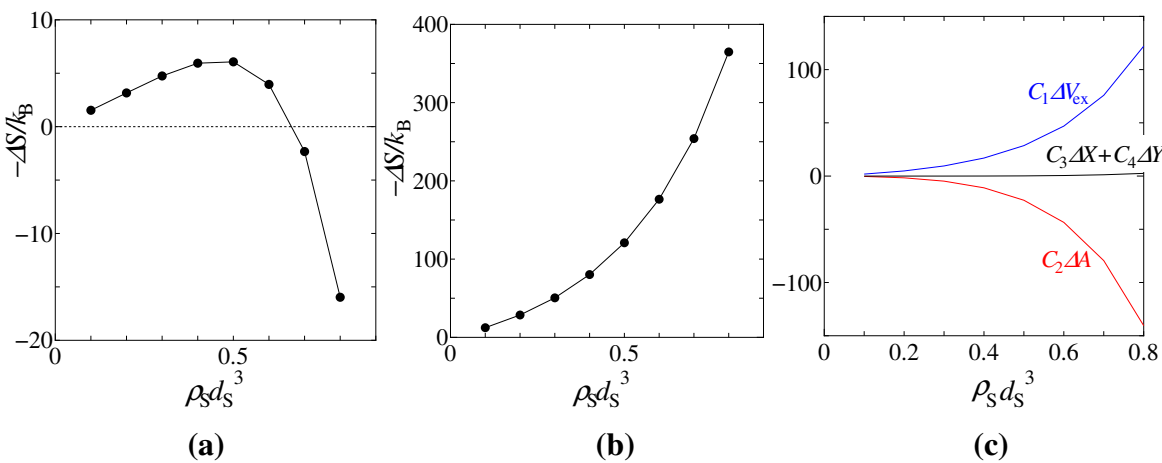
We consider $-\Delta S/k_B = (-S/k_B)^{Unfold} - \{(-S/k_B)^{Native}\}$ where the superscripts “Native” and “Unfold” represent the values for the native structure and for an unfolded structure of protein G, respectively ($C_3X + C_4Y$ is fully incorporated here). All structures are the same as those shown in Table 1. In the present hard-sphere model, $-\Delta S/k_B$ corresponds to the change in μ upon the transition from the native structure to an unfolded one. Figure 4(a) shows $-\Delta S/k_B$ upon the structural transition to the swelling structure. As the density corresponding to the pressure increases, the swelling structure becomes more destabilized than the native structure in the low-pressure region. This is because C_1 is much larger than $|C_2|$, with the result that any structure with larger EV is more destabilized. However, as the density increases further, it begins to decrease rather rapidly and they eventually turn more stable than the native structure. The change in the PMV upon the structural transition is 117 \AA^3 at $\rho_{SDS}^3 = 0.2$ and -195 \AA^3 at $\rho_{SDS}^3 = 0.8$, respectively. According to the experimental results [61], the volume change upon protein unfolding is positive at low pressures and negative at high pressures. Therefore, the present results are consistent with the experimental ones. The swelling structure can be regarded as the pressure-induced structure.

We also show $-\Delta S/k_B$ upon the structural transition to the random-coil structures in Figure 4(b). The SE of the random-coil structures is taken to be the average value calculated for the 32 random coils [62]. It follows that $-\Delta S/k_B$ continues to increase upon raising density and thus the random-coil structures are unstable even for the high densities. The change in the PMV upon the structural

transition to the random-coil structures is 464 \AA^3 at $\rho_S d_S^3 = 0.8$ and is positive value. Therefore, the random-coil structure is not a pressure-induced one.

We now discuss the physical origin of the structural transition from the native structure to the swelling structure occurring at high pressures. The decomposition of $-\Delta S/k_B$ into $C_1\Delta V_{\text{ex}}$, $C_2\Delta A$, and $C_3\Delta X + C_4\Delta Y$ in the case of Figure 4(a) is shown in Figure 4(c). The term $C_1\Delta V_{\text{ex}}$ is positive and increases as the solvent density becomes higher. The term $C_3\Delta X + C_4\Delta Y$ is also positive and is much smaller than the other two terms. Therefore, these terms prevent the transition. The structural transition comes primarily from the ASA term ($C_2\Delta A$) which is negative and decreases further as the density becomes higher. In the case of the random-coil structures where both of the EV and the ASA are much larger than those of the native structure (see Table 1), although their ASA term takes a very large negative value, $-\Delta S/k_B$ is still positive due to the even larger positive value of the EV term ($C_1\Delta V_{\text{ex}}$). Therefore, inversion of the relative stability occurs for the swelling structure because its ASA is considerably larger and its EV is only moderately larger than the native structure (see Table 1).

Figure 4. Negative of the entropy change of solvent scaled by k_B upon the transition from the native structure to (a) the swelling structure and (b) the random-coil structures of protein G plotted against the bulk solvent density corresponding to the pressure P . $-\Delta S/k_B = (-S/k_B)^{\text{Unfold}} - \{(-S/k_B)^{\text{Native}}\}$ where the superscripts “Native” and “Unfold” represent the values for the native structure and for the unfolded structure, respectively. (c) Decomposition of $-\Delta S/k_B$ for swelling structure of protein G [Figure 4(a)] into $C_1\Delta V_{\text{ex}}$, $C_2\Delta A$, and $C_3\Delta X + C_4\Delta Y$ at each bulk solvent density.



4.2. Pressure-induced Helix-coil Transition of a Polypeptide

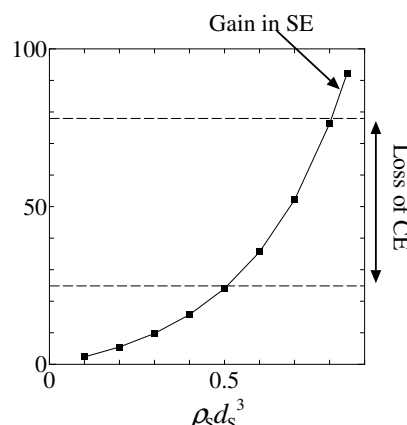
We have recently proposed a physical picture to explain the pressure-induced helix-coil transition obtained experimentally by Kato *et al.* [41]. We first discuss the changes in the solvent entropy and the conformational entropy of the polypeptide upon the transition from the coil state to the helix state. Hereafter $\Delta S = S^{\text{Helix}} - S^{\text{Coil}}$ and $\Delta S_C = S_C^{\text{Helix}} - S_C^{\text{Coil}}$ denote the changes in the solvent entropy and in the conformational entropy upon the transition from the coil state to the helix state, respectively. The superscripts “Helix” and “Coil” represent the values for the helix state and for the coil state, respectively.

As explained in Section 2, the loss of the conformational entropy, $|\Delta S_C|$, is expected to be independent of the pressure or decreasing function of the pressure. We assume that ΔS_C is independent of the pressure hereafter. The pressure-induced helix-coil transition of a polypeptide [17,18] can be understood by the structural stability described by the competition between the solvent-entropy gain and the conformational-entropy loss of the polypeptide upon the transition [41]. At low pressures, ΔS is smaller than $|\Delta S_C|$ and the coil state is stabilized. However, since ΔS is a monotonically increasing function of the pressure [see Figure 4(b)], the inversion occurs at a sufficiently high pressure, leading to the transition from the coil state to the helix state.

We calculate $\Delta S/k_B$ and $\Delta V_{PMV} = V_{PMV}^{\text{Helix}} - V_{PMV}^{\text{Coil}}$ using the morphometric approach to show the validity of this physical picture [41] (C_3X+C_4Y is fully incorporated here). The polypeptide we consider is composed of 20 alanine residues. The hard-body model described in Section 3.1 is employed. We assume that the helix state is represented by a complete α -helix structure and that the coil state is an ensemble of random coils. Random coil structures are generated by assigning a random number to the dihedral angles for the main chain [62]. The SE and the PMV of the coil state are taken to be the average value of those for the nine random coils generated. We estimate the range of $\Delta S_C/k_B$ using the method described in Section 3.3. Since N_r is 20, the actual CE loss should lie in the range, $24.9 < |\Delta S_C/k_B| < 78.0$.

Figure 5 shows the solvent-density dependence (corresponding to the pressure dependence) of the solvent-entropy gain, $\Delta S/k_B$, and the conformational-entropy loss, $|\Delta S_C/k_B|$, upon the transition from the coil state to the helix state. At low densities $\Delta S/k_B$ is smaller than the lower limit of $|\Delta S_C/k_B|$ and thus the polypeptide is in the coil state. On the other hand, $\Delta S/k_B$ prevails over the upper limit of $|\Delta S_C/k_B|$ at sufficiently high densities. Therefore, the transition from the coil state to the complete α -helix structure occurs. The change in the PMV upon the transition, ΔV_{PMV} , is -134 \AA^3 at $\rho_S d_s^3 = 0.7$ and is negative value. The experimental results by Kato *et al.* [17,18] have thus been reproduced qualitatively. Even when the conformational-entropy loss is assumed to be a decreasing function of the pressure, our conclusions are not altered: The transition occurs simply at a slightly lower solvent density.

Figure 5. ΔS and $|\Delta S_C|$ plotted against the bulk solvent density corresponding to the pressure. $|\Delta S_C|$ lies between the two dashed lines. The SE gain and the CE loss upon the transition from the coil state (an ensemble of random coils) to the complete α -helix structure are compared.



Though the pressure-induced transition from the coil state to the helix state for the polypeptide appears to be inconsistent with pressure denaturation of a protein and the dissociation of the protein complex caused at high pressures, they can be elucidated in terms of the translational entropy of water. The apparent inconsistency arises partly from the difference in a number of residues, N_r . For the polypeptide whose N_r is very small, as shown by Harano and Kinoshita [24], at low pressures the solvent entropy gain cannot prevail the conformational-entropy loss and the peptide takes the coil state. On the other hand, a protein with large N_r folds into the native structure even at low pressures because the solvent-entropy gain dominates [24]. As shown in Figure 4(b), the native structure becomes more stable than the random coil structure at high pressures.

Here we discuss why the polypeptide adopts the helix structure at high pressures, although there are many compact structures. The recent analyses of a protein have shown that the complete helix structure also possesses the characteristics of the pressure-induced structure [63]. The complete helix structure can be the most stable at high pressures as in the case of the alanine-based peptide, too. Therefore, we can conclude that both of protein and polypeptide take the pressure-induced structure at high pressures.

We consider only the entropic component with the neglect of the energetic component. Here we discuss the pressure dependence of energy change upon the helix-coil transition. When the transition occurs, a very large gain of the polypeptide intramolecular energy occurs due to the formation of intramolecular hydrogen bonds and van der Waals attractive interactions between polypeptide atoms. However, the transition accompanies serious dehydration. The dehydration means the break of hydrogen bonds between water oxygen and polypeptide oxygen or nitrogen (hereafter, this is referred to as "hydrogen bonds with water molecules") and the loss of van der Waals attractive interactions between polypeptide atoms and water oxygen or hydrogen (or either of the break or the loss). At least within a framework of classical mechanics, the intramolecular-energy change is independent of the pressure. We have recently analyzed the pressure dependence of the hydration energy for hydrophobic and hydrophilic solutes using the angle-dependent integral equation theory combined with the multipolar water model. It is found that the hydration energy always decreases as the pressure becomes higher (we are planning to report this result in a forthcoming paper.) In particular, the exposed hydrophilic solutes are energetically more stabilized due to enhanced hydrogen bonds or an increase in the number of hydrogen bonds with water molecules. The analysis indicates that the energy loss by the break of the interaction between polypeptide atoms and water molecule is increased with raising pressure. Thus, the energy change upon the coil-to-helix transition increases with raising pressures and it may become eventually positive at high pressures. Therefore, the energetic component prevents the transition. The transition is induced only by the solvent entropy in the entropic component.

4.3. Comment on Formation/Dissociation Process of Amyloid Fibrils

It is experimentally known that the amyloid fibrils are dissociated into monomers when a high pressure is applied to the system [7-9]. We discuss this experimental observation using Equation (10). "High" and "Low" denote monomers and fibrils, respectively. According to experimental results, there are lots of vacant spaces within the fibrils, which water molecules cannot enter [64] (we emphasize that even with such small vacant spaces, overlaps of the excluded volumes generated by protein subunits certainly occur, and the EV of the fibrils is smaller than that of the monomers). Due to the small

vacancies, $V_{\text{ex}}^{\text{Low}}$ is significantly large while A^{Low} is fairly small. Therefore, upon the dissolution of the amyloid fibrils, $V_{\text{ex}}^{\text{High}} - V_{\text{ex}}^{\text{Low}}$ can be kept sufficiently small, even though $A^{\text{High}} - A^{\text{Low}}$ becomes quite large. The dissolution to monomers whose structures feature like pressure-induced ones can be the best solution. The monomers cannot be random coils because of the unacceptably large EV-increase despite the largest ASA-increase. The dissolution of the other protein complexes can be understood in a similar manner. Thus, the folding/unfolding transition of a protein and the formation/dissociation process of amyloid fibrils can be discussed within the same framework, pending theoretical verification in future studies for the latter.

5. Conclusions

We have reviewed the general framework of pressure effects on structures formed by entropically driven self-assembly. At low pressures, the structures almost minimizing the EV generated for solvent particles are stabilized. Such structures appear to be even more stabilized at high pressures. However, it is experimentally known that the native structure of a protein is unfolded and ordered aggregates such as amyloid fibrils and virus assemblies are dissolved by applying high pressures. A clue to the basic mechanism is in the phenomenon that when a large hard-sphere solute is immersed in small hard spheres forming the solvent, the small hard spheres are enriched near the solute and this enrichment becomes greater as the pressure increases. We have argued that “attraction” is entropically provided between the solute surface and solvent particles and the attraction becomes higher with rising pressure. Due to this effect, at high pressures, the structures possessing the largest possible solvent-accessible surface area together with sufficiently small EV turn more stable in terms of the solvent entropy.

Two examples—pressure denaturation of proteins and pressure-induced helix-coil transition of a polypeptide—have been discussed to show the validity of the picture. By an analysis of the pressure denaturation for illustrating our framework, only a class of special structures is shown to turn more stabilized relative to the native structure at sufficiently high pressures. Those structures are characterized by only moderately larger EV and much larger ASA, which is attained by the solvent penetration into the protein interior. We have also shown that the pressure-induced helix-coil transition of a polypeptide, which appears to be inconsistent with pressure denaturation or dissociation caused at high pressures known for many proteins, can also be explained in terms of the solvent entropy. At sufficiently high pressures, the stabilized structures for both of the peptide and the protein are compact and characterized by the largest possible ASA together with the EV kept sufficiently small. We have also commented how the amyloid fibrils are dissolved at high pressures on the basis of the solvent entropy.

In the present review, we have been concentrated on the translational entropy of water. The other terms (intramolecular and solvation energy and conformational entropy), which prevent denaturation and dissociation, are ignored. This is because the aim of the present study is to elucidate the microscopic mechanism of pressure effects on the structures formed by entropically driven self-assembly. The factor which prevents denaturation and dissociation is not necessary for the present aim. On the other hand, if we intend to predict quantitatively the pressure at which pressure denaturation occurs, or to perform a quantitative comparison with the experimental result, the other terms are needed. Namely, we need to discuss in terms of the free-energy change.

We have employed the hard-body model to focus on the water-entropic effect. This model is useful for qualitative discussions of many cases such as protein folding and pressure denaturation of proteins discussed here. However, even when the translational entropy of water is the key factor, modeling water molecules as hard spheres fails when we wish to elucidate the microscopic mechanism of cold denaturation of a protein [65,66] and to obtain quantitatively reliable results [25]. It is also impossible to analyze the hydration of ions using the hard sphere as a solvent. In these cases, multipolar water model [50,51] is suitable.

It has been shown that the translational entropy of water is the key quantity for cold [65,66] and heat [67] denaturations of proteins and the prediction of the native structure [68–70] as well as protein folding and pressure denaturation of proteins discussed here. We have recently reported a new progress in elucidating the mechanism of the unidirectional movement of a linear-motor protein (e.g., myosin) along a filament (e.g., F-actin) [71] and the rotation mechanism of F₁-ATPase [72]. Therefore, it should be emphasized that the water-entropy effect is imperative for a variety of self-assembling and aggregation processes in biological systems sustaining life.

Acknowledgements

The author thanks Profs. Masahiro Kinoshita and Yuichi Harano for their collaboration. The development of the computer program for the morphometric approach was made possible by them and Dr. Roland Roth, whose useful comments are greatly appreciated. This work was supported by Innovative Areas (Grant No. 20118004) from the Ministry of Education, Culture, Sports, Science and Technology of Japan and by the Next Generation Super Computing Project, Nanoscience Program, MEXT, Japan.

References and Notes

1. Dobson, C.M. Protein folding and misfolding. *Nature* **2003**, *426*, 884–890.
2. Panick, G.; Malessa, R.; Winter, R.; Rapp, G.; Frye, K.J.; Royer, C.A. Structural characterization of the pressure-denatured state and unfolding/refolding kinetics of staphylococcal nuclease by synchrotron small-angle X-ray scattering and Fouriertransform infrared spectroscopy. *J. Mol. Biol.* **1998**, *275*, 389–402.
3. Royer, C.A. Revisiting volume changes in pressure-induced protein unfolding. *Biochim. Biophys. Acta* **2002**, *1575*, 201–209.
4. Lesch, H.; Schlichter, J.; Friedrich, J.; Vanderkooi, J.M. Molecular probes: what is the range of their interaction with the environment? *Biophys. J.* **2004**, *86*, 467–472.
5. Paliwal, A.; Asthagiri, D.; Bossev, D.P.; Paulaitis, M.E. Pressure denaturation of staphylococcal nuclease studied by neutron small-angle scattering and molecular simulation. *Biophys. J.* **2004**, *87*, 3479–3492.
6. Meersman, F.; Dobson, C.M.; Heremans, K. Protein unfolding, amyloid fibril formation and configurational energy landscapes under high pressure conditions. *Chem. Soc. Rev.* **2006**, *35*, 908–917.
7. Foguel, D.; Suarez, M.C.; Ferrao-Gonzales, A.D.; Porto, T.C.R.; Palmieri, L.; Einsiedler, C.M.; Andrade, L.R.; Lashuel, H.A.; Lansbury, P.T.; Kelly, J.W.; Silva, J.L. Dissociation of amyloid

- fibrils of α -synuclein and transthyretin by pressure reveals their reversible nature and the formation of water-excluded cavities. *Proc. Natl. Acad. Sci. USA* **2003**, *100*, 9831-9836.
- 8. Meersman, F.; Dobson, C.M. Probing the pressure-temperature stability of amyloid fibrils provides new insights into their molecular properties. *Biochim. Biophys. Acta.* **2006**, *1764*, 452-460.
 - 9. Mishra, R.; Winter, R. Cold- and pressure-induced dissociation of protein aggregates and amyloid fibrils. *Angew. Chem. Int. Ed.* **2008**, *47*, 6518-6521.
 - 10. Bonafe, C.F.; Vital, C.M.; Telles, R.C.; Goncalves, M.C.; Matsuura, M.S.; Pessine, F.B.; Freitas, D.R.; Vega, J. Tobacco mosaic virus disassembly by high hydrostatic pressure in combination with urea and low temperature. *Biochemistry* **1998**, *37*, 11097-11105.
 - 11. Latif, A.R.A.; Kono, R.; Tachibana, H.; Akasaka, K. Kinetic analysis of amyloid protofibril dissociation and volumetric properties of the transition state. *Biophys. J.* **2007**, *92*, 323-329.
 - 12. Kitahara, R.; Yokoyama, S.; Akasaka, K. NMR snapshots of a fluctuating protein structure: Ubiquitin at 30 bar-3 kbar. *J. Mol. Biol.* **2005**, *347*, 277-285.
 - 13. Collins, M.D.; Hummer, G.; Quillin, M.L.; Matthews, B.W.; Gruner, S.M. Cooperative water filling of a nonpolar protein cavity observed by high-pressure crystallography and simulation. *Proc. Natl. Acad. Sci. USA* **2005**, *102*, 16668-16671.
 - 14. Day, R.; Garcia, A.E. Water penetration in the low and high pressure native states of ubiquitin. *Proteins Struct. Funct. Genet.* **2008**, *70*, 1175-1184.
 - 15. Imai, T.; Sugita, Y. Dynamic correlation between pressure-induced protein structural transition and water penetration. *J. Phys. Chem. B.* **2010**, *114*, 2281-2286.
 - 16. Hummer, G.; Garde, S.; Garcia, A.E.; Paulaitis, M.E.; Pratt, L.R. The pressure dependence of hydrophobic interactions is consistent with the observed pressure denaturation of proteins. *Proc. Natl. Acad. Sci. USA* **1998**, *95*, 1552-1555.
 - 17. Takekiyo, T.; Shimizu, A.; Kato, M.; Taniguchi, Y. Pressure-tuning FT-IR spectroscopic study on the helix-coil transition of Ala-rich oligopeptide in aqueous solution. *Biochim. Biophys. Acta.* **2005**, *1750*, 1-4.
 - 18. Imamura, H.; Kato, M. Effect of pressure on helix-coil transition of an alanine-based peptide: An FT-IR study. *Proteins: Struct. Funct. Genet.* **2009**, *75*, 911-918.
 - 19. Paschek, D.; Gnanakaran, S.; Garcia, A.E. Simulations of the pressure and temperature unfolding of an α -helical peptide. *Proc. Natl. Sci. USA* **2005**, *102*, 6765-6770.
 - 20. Paschek, D.; Garcia, A.E. Reversible temperature and pressure denaturation of a protein fragment: A replica exchange molecular dynamics simulation study. *Phys. Rev. Lett.* **2004**, *93*, 238105.
 - 21. Kauzmann, W. Some factors in the interpretation of protein denaturation. *Adv. Protein Chem.* **1959**, *14*, 1-63.
 - 22. Lee, B.; Richards, F.M. The interpretation of protein structures: estimation of static accessibility. *J. Mol. Biol.* **1971**, *55*, 379-400.
 - 23. Harano, Y.; Kinoshita, M. Large gain in translational entropy of water is a major driving force in protein folding. *Chem. Phys. Lett.* **2004**, *399*, 342-348.
 - 24. Harano, Y.; Kinoshita, M. Translational-entropy gain of solvent upon protein folding. *Biophys. J.* **2005**, *89*, 2701-2710.

25. Yoshidome, T.; Kinoshita, M.; Hirota, S.; Baden, N.; Terazima, M. Thermodynamics of apoplastocyanin folding: Comparison between experimental and theoretical results. *J. Chem. Phys.* **2008**, *128*, 225104.
26. Kinoshita, M. Importance of translational entropy of water in biological self-assembly processes like protein folding. *Int. J. Mol. Sci.* **2009**, *10*, 1064-1080.
27. Kinoshita, M. Roles of translational motion of water molecules in sustaining life. *Front. Biosci.* **2009**, *14*, 3419-3454.
28. Yasuda, S.; Yoshidome, T.; Oshima, H.; Kodama, R.; Harano, Y.; Kinoshita, M. Effects of side-chain packing on the formation of secondary structures in protein folding. *J. Chem. Phys.* **2010**, *132*, 065105.
29. Kinoshita, M. Spatial distribution of a depletion potential between a big solute of arbitrary geometry and a big sphere immersed in small spheres. *J. Chem. Phys.* **2002**, *116*, 3493-3501.
30. Kinoshita, M. Roles of entropic excluded-volume effects in colloidal and biological systems: Analyses using the three-dimensional integral equation theory. *Chem. Eng. Sci.* **2006**, *61*, 2150-2160.
31. Kinoshita, M. Interaction between big bodies with high asphericity immersed in small spheres. *Chem. Phys. Lett.* **2004**, *387*, 47-53.
32. Kinoshita, M. Ordered aggregation of big bodies with high asphericity in small spheres: A possible mechanism of the amyloid fibril formation. *Chem. Phys. Lett.* **2004**, *387*, 54-60.
33. Baden, N.; Hirota, S.; Takabe, T.; Funasaki, N.; Terazima, M. Thermodynamical properties of reaction intermediates during apoplastocyanin folding in time-domain. *J. Chem. Phys.* **2007**, *127*, 175103.
34. Ohtaka, H.; Schon, A.; Freire, E. Multidrug Resistance to HIV-1 Protease Inhibition Requires Cooperative Coupling between Distal Mutations. *Biochemistry* **2003**, *42*, 13659-13666.
35. Kardos, J.; Yamamoto, K.; Hasegawa, K.; Naiki, H.; Goto, Y. Direct measurement of the thermodynamic parameters of amyloid formation by isothermal titration calorimetry. *J. Biol. Chem.* **2004**, *279*, 55308-55314.
36. Kasai, M.; Asakura, S.; Oosawa, F. The G-F equilibrium in actin solutions under various conditions. *Biochim. Biophys. Acta.* **1962**, *57*, 13-21.
37. Swezey, R.R.; Somero, G.N. Polymerization thermodynamics and structural stabilities of skeletal muscle actins from vertebrates adapted to different temperatures and hydrostatic pressures. *Biochemistry* **1982**, *21*, 4496-4503.
38. Yoshidome, T.; Harano, Y.; Kinoshita, M. Pressure effects on structures formed by the entropically driven self-assembly: Illustration for denaturation of proteins. *Phys. Rev. E.* **2009**, *79*, 011912.
39. Harano, Y.; Kinoshita, M. On the physics of pressure denaturation of proteins. *J. Phys. Condens. Matter.* **2006**, *18*, L107-L113.
40. Harano, Y.; Kinoshita, M. Crucial importance of translational entropy of water in pressure denaturation of proteins. *J. Chem. Phys.* **2006**, *125*, 024910.
41. Yoshidome, T.; Kinoshita, M. Pressure effect on helix-coil transition of an alanine-based peptide: Theoretical analysis. *Chem. Phys. Lett.* **2009**, *477*, 211-215.

42. Harano, Y.; Yoshidome, T.; Kinoshita, M. Molecular mechanism of pressure denaturation of proteins. *J. Chem. Phys.* **2008**, *129*, 145103.
43. Hansen, J.P.; McDonald, L.R. *Theory of Simple Liquids*; Academic Press: London, UK, 1986.
44. Asakura, S.; Oosawa, F. On interaction between two bodies immersed in a solution of macromolecules. *J. Chem. Phys.* **1954**, *22*, 1255-1256.
45. Asakura, S.; Oosawa, F. Interaction between particles suspended in solutions of macromolecules. *J. Polymer Sci.* **1958**, *33*, 183-192.
46. Imai, T.; Harano, Y.; Kinoshita, M.; Kovalenko, A.; Hirata, F. A theoretical analysis on hydration thermodynamics of proteins. *J. Chem. Phys.* **2006**, *125*, 024911.
47. Ikeguchi, M.; Doi, J. Direct numerical solution of the Ornstein-Zernike integral equation and spatial distribution of water around hydrophobic molecules. *J. Chem. Phys.* **1995**, *103*, 5011-5017.
48. Kinoshita, M. Molecular origin of the hydrophobic effect: Analysis using the angle-dependent integral equation theory. *J. Chem. Phys.* **2008**, *128*, 024507.
49. Kinoshita, M.; Yoshidome, T. Molecular origin of the negative heat capacity of hydrophilic hydration. *J. Chem. Phys.* **2009**, *130*, 144705.
50. Kusalik, P.G.; Patey, G.N. On the molecular theory of aqueous electrolyte solutions. I. The solution of the RHNC approximation for models at finite concentration. *J. Chem. Phys.* **1988**, *88*, 7715-7738.
51. Kusalik, P.G.; Patey, G.N. The solution of the reference hypernetted-chain approximation for water-like models. *Mol. Phys.* **1988**, *65*, 1105-1119.
52. Kirkwood, J.G.; Buff, F.P. The statistical mechanical theory of solutions. I. *J. Chem. Phys.* **1951**, *19*, 774-777.
53. König, P.M.; Roth, R.; Mecke, K.R. Morphological thermodynamics of fluids: Shape dependence of free energies. *Phys. Rev. Lett.* **2004**, *93*, 160601.
54. Roth, R.; Harano, Y.; Kinoshita, M. Morphometric approach to the solvation free energy of complex molecules. *Phys. Rev. Lett.* **2006**, *97*, 078101.
55. Morita, T. Theory of classical fluids: Hyper-netted chain approximation. III: a New Integral Equation for the Pair Distribution Function. *Prog. Theor. Phys.* **1960**, *23*, 829-845.
56. Morita, T.; Hiroike, K. A new approach of the theory of classical fluids. Part III: General treatment of classical systems. *Prog. Theor. Phys.* **1961**, *25*, 537-578.
57. Berendsen, H.J.C.; Grigera, J.R.; Straatsma, T.P. The missing term in effective pair potentials. *J. Phys. Chem.* **1987**, *91*, 6269-6271.
58. Doig, A.J.; Sternberg, M.J.E. Side-chain conformational entropy in protein folding. *Prot. Sci.* **1995**, *4*, 2247-2251.
59. Fitter, J. A measure of conformational entropy change during thermal protein unfolding using neutron spectroscopy. *Biophys. J.* **2003**, *84*, 3924-3930.
60. Dill, K.A.; Ozkan, S.B.; Shell, M.S.; Weikl, T.R. The protein folding problem. *Annu. Rev. Biophys.* **2008**, *37*, 289-316.
61. Kauzmann, W. Thermodynamics of unfolding. *Nature* **1987**, *325*, 763-764.

62. Imai, T.; Harano, Y.; Kinoshita, M.; Kovalenko, A.; Hirata, F. Theoretical analysis on changes in thermodynamic quantities upon protein folding: Essential role of hydration. *J. Chem. Phys.* **2007**, *126*, 225102.
63. We expect that the structural transition from the native structure to the complete-helix structure is very difficult because large conformational change from the native structure is necessary.
64. Akasaka, K.; Latif, A.R.A.; Nakamura, A.; Matsuo, K.; Tachibana, H.; Gekko, K. Amyloid protofibril is highly voluminous and compressible. *Biochemistry* **2007**, *46*, 10444-10450.
65. Yoshidome, T.; Kinoshita, M. Hydrophobicity at low temperatures and cold denaturation of a protein. *Phys. Rev. E* **2009**, *79*, 030905.
66. Oshima, H.; Yoshidome, T.; Amano, K.; Kinoshita, M. A theoretical analysis on characteristics of protein structures induced by cold denaturation. *J. Chem. Phys.* **2009**, *131*, 205102.
67. Amano, K.; Yoshidome, T.; Harano, Y.; Oda, K.; Kinoshita, M. Theoretical analysis on thermal stability of a protein focused on the water entropy. *Chem. Phys. Lett.* **2009**, *474*, 190-194.
68. Harano, Y.; Roth, R.; Kinoshita, M. On the energetics of protein folding in aqueous solution. *Chem. Phys. Lett.* **2006**, *432*, 275-280.
69. Harano, Y.; Roth, R.; Sugita, Y.; Ikeguchi, M.; Kinoshita, M. Physical basis for characterizing native structures of proteins. *Chem. Phys. Lett.* **2007**, *437*, 112-116.
70. Yoshidome, T.; Oda, K.; Harano, Y.; Roth, R.; Sugita, Y.; Ikeguchi, M.; Kinoshita, M. Free-energy function based on an all-atom model for proteins. *Proteins Struct. Funct. Genet.* **2009**, *77*, 950-961.
71. Amano, K.; Yoshidome, T.; Iwaki, M.; Suzuki, M.; Kinoshita, M. Entropic potential field formed for a linear-motor protein near a filament: Statistical-mechanical analyses using simple models. *J. Chem. Phys.* in press.
72. Yoshidome, T.; Ito, Y.; Ikeguchi, M.; Kinoshita, M. On the Rotation Mechanism of F₁-ATPase: Crucial Importance of Water-Entropy Effect. *J. Am. Chem. Soc.* submitted.

© 2010 by the authors; licensee MDPI, Basel, Switzerland. This article is an Open Access article distributed under the terms and conditions of the Creative Commons Attribution license (<http://creativecommons.org/licenses/by/3.0/>).